Supplementary Information for

Six hundred years of South American tree rings reveal an increase in severe hydroclimatic events since mid-20th century

Mariano S. Morales, Edward R. Cook, Jonathan Barichivich, Duncan A. Christie, Ricardo Villalba, Carlos LeQuesne, Ana M. Srur, María E. Ferrero, Álvaro González-Reyes, Fleur Couvreux, Vladimir Matskovsky, Juan C. Aravena, Antonio Lara, Ignacio A. Mundo, Facundo Rojas, María R. Prieto, Jason E. Smerdon, Lucas O. Bianchi, Mariano H. Masiokas, Rocio Urrutia-Jalabert, Milagros Rodriguez-Catón, Ariel A. Muñoz, Moises Rojas-Badilla, Claudio Alvarez, Lidio Lopez, Brian H. Luckman, David Lister, Ian Harris, Philip D. Jones, A. Park Williams, Gonzalo Velazquez, Diego Aliste, Isabella Aguilera-Betti, Eugenia Marcotti, Felipe Flores, Tomás Muñoz, Emilio Cuq, José A. Boninsegna

Mariano S. Morales
Email: mmorales@mendoza-conicet.gob.ar

This PDF file includes:

This Supplementary Information has the following sections:
1. Instrumental data set
2. Developing the instrumental scPDSI data set
3. SADA tree ring network
4. Standardizing SADA tree ring chronologies:
5. Point by point regression: the drought reconstruction method
6. Calibration and verification statistics of the reconstruction model
7. Queens Case Imputation and Smoothing (QCIS)
8. Historical hydroclimate reconstructions
9. Changes in extremes in South America regions
10. Large-scale ocean-atmosphere climate datasets (SST, SST_N3.4, GPH500 and SAM)
11. Maximum Covariance Analysis for instrumental scPDSI and climate drivers
12. Comparisons to other ENSO and SAM reconstructions

One table, ten figures and three datasets accompany these sections and are referred to by them.
Table S1
Figs. S1 to S10

Legends for Datasets S1 to S3
SI References

www.pnas.org/cgi/doi/10.1073/pnas.2002411117

Other supplementary materials for this manuscript include the following:

Datasets S1 to S3

Here we provide additional information regarding the SADA development and its validation.

1. Instrumental data set.

The global database of climate variables is based mostly on National Meteorological Services (NMS) meteorological stations with few high-altitude stations in remote areas with complex topographies, such as the Andes. To tackle these deficiencies we developed a monthly climate database by compiling records from hundreds of high-altitude meteorological stations from different institutional sources in addition to those from the NMS. Based on these data we developed an instrumental database of 992 precipitation and 292 temperature records (IANIGLA database), spatially distributed throughout the Andes between 12º and 56ºS latitude. The meteorological records were changed to a common format and quality checked based as described below.
Monthly temperature anomalies were accepted if they met the following criteria:

1- $(T - T_{clim}) < 3$ sigma
2- $(T - T_{clim}) < T_{clim}+5ºC$

Where T= monthly temperature anomalies; T_{clim}= historic mean of monthly tempeture.
Monthly precipitation anomalies were accepted which met the criteria

1- $(Pr - Pr_{clim}) < 3$ sigma
2- $(Pr - Pr_{clim}) < Pr_{clim} \times 5$
3- $Pr-Pr_{clim} < 100mm$

Where Pr= total monthly precipitation anomalies; Pr_{clim}= historic mean of the monthly precipitation.

For those cases in which these conditions were not met and extreme values were present, a visual examination and comparison with neighboring stations was applied to determine whether the extreme matched the regional climate pattern. If not, the monthly data point was removed from the database. To create longer and more complete series, we merged the final versions of the series with matching series from the monthly data set compiled by the Climatic Research Unit Time Series (CRU TS 3.24) (1). The resulting merger and addition of the new dataset was included in later versions of CRU TS (such as CRU TS 4.03). Figure S1 shows maps by decade for the period 1901-2000 of the changing density of precipitation stations available for interpolation onto the CRU TS 3.24 + IANIGLA database precipitation field. There is an obvious loss of local precipitation data for interpolation prior to 1950, particularly in southern Patagonia, northern Chile, northeastern Argentina, Bolivia, Paraguay, Uruguay, southern Brazil and southern Peru (Fig. S1). The gridding methodology in areas devoid of stations produces a loss of variance in the CRU dataset, otherwise referred to as “relaxation to climatology” (2).
To develop a more complete and parsimonious instrumental dataset, an ensemble of the interpolated fields of monthly total precipitation, temperatures (mean, maximum, minimum), and potential evapotranspiration observations was produced from three climate databases. The employed databases were: 1) precipitation, temperature, and potential evapotranspiration data from the CRU TS 3.24, University of East Anglia (1), enhanced by the incorporation of precipitation and temperature records from the National Institute of Snow Glaciology and Environmental Sciences (IANIGLA-CONICET) database; 2) precipitation and air temperature

datasets from the University of Delaware (3); and 3) the precipitation dataset from the Global Precipitation Climatology Centre (GPCC) (4).
Figure S2 shows the correlation between the CRU TS 3.24 DJF precipitation dataset and the ensemble dataset of this study for three periods: A) 1901-2015, B) 1901-1950, and C) 1951-2015. A clear decrease in the correlation coefficients over the Andes is observed during the three periods as a result of the lack of stations in these areas in the CRU_TS 3.24 data set. In particular, poor correlations appear in southern Bolivia and the Andean Cordillera during the period 1901-1950 (Fig. S2b). The climate data ensemble produced by incorporation of the IANIGLA instrumental database represents a significant improvement over the original CRU TS database because it increases the density of high-altitude meteorological stations. Nevertheless, even in the ensemble precipitation dataset there are still signficantly under-represented regions in the Andes, southern Bolivia, and southern Patagonia, especially prior to 1951. A similar reduction in meteorological station coverage before 1951 was noted over China during the development of the Monsoon Asia Drought Atlas (MADA; 5). This led to the decision to begin the MADA calibration period in 1951 in order to use the highest quality instrumental data for developing the pointwise reconstruction models. The same choice based on a similar argument has been made here for production of the SADA.

2. Developing the instrumental scPDSI data set.
The scPDSI (6) is calculated from time series of precipitation and temperature, together with the estimated potential evapotranspiration (PET, see references in 1). In this study instrumental monthly scPDSI was computed following Wells et al. (6) for the period 1901-2015. One-half degree gridded monthly scPDSI was the target field used for reconstruction. The monthly instrumental scPDSI data were seasonalized to produce austral summer (DJF) average values to be used for tree-ring based reconstruction at each grid point. Summer is the principal growing season of trees and was also the season targeted in the other drought atlases (NADA, MADA, OWDA, ANZDA, MXDA, ERDA).

3. SADA tree-ring network.
286 tree ring chronologies have been developed, mostly concentrated on both sides of the Andes Cordillera (16º-56ºS), from the Altiplano and intermontane subtropical valleys to the Patagonian forests at the southern tip of the continent (Table S1; Fig S3). New collections in tropical lowlands have additionally allowed extension of the geographical coverage of tree ring records to lower latitudes and elevations. Figure S3, shows the network of 286 annual tree ring chronologies. The length of the target period (1400-2000 C.E.) for reconstruction of scPDSI results from the presence of a relatively high number of tree ring chronologies and good spatial coverage along the Andes. Sixty-five of these tree ring chronologies completely cover the 15th century and are well distributed throughout the Altiplano, central Chile, and Northern Patagonia (Fig. S3). The number and the spatial coverage of the tree ring chronologies increase during the following centuries, providing an adequate network to reconstruct regional South American hydroclimate for the past six centuries.

4. Standardizing SADA tree ring chronologies.
The tree ring chronologies used for reconstruction were standardized (7) to remove biological growth trends related to increasing tree size and age and to render the interannual changes in radial growth stationary over time. This process of detrending and transformation of the basic raw tree ring measurements results in a set of dimensionless growth indices with a defined mean of 1.0 and a standard deviation related in part to the strength of the primary climate signal contained in the indices. This allows the standardized indices from many samples to be averaged into a single tree ring chronology at a specific site for climate reconstruction. There are 286 of these site chronologies in the SADA tree ring network.
The detrending method is a key step in preparing tree ring series for climate reconstruction, but it can also remove low and medium frequency climate-related variance from centennial to millennial-length tree ring series. This is related in part to the 'segment length curse' (8), because

it is not possible to retain low frequency variability in data that is longer than the tree ring series being detrended. Additionally, the different growth curve methods used in detrending can have strong effects on the retention of low-to-medium frequency variance due to climate. The signal-free (SF) method (9) minimizes trend distortion artifacts, principally at the ends of the series being detrended, and recovers common medium-to-low frequency variability throughout the length of the tree ring chronology that may have been inadvertently removed by the detrending curves as initially applied. This cannot be done in one step because the trend distortion artifacts and lost common variance are not known at the start. Rather, the SF is an iterative procedure that is applied to the raw tree ring measurements until no change in the final site chronology is detected. See Melvin and Briffa (9) for details. Thus, SF is an iterative detrending method that can potentially protect from the loss of common low-to-medium frequency variability caused by traditional detrending methods (e.g., 7). However, different curve fits in combination with SF can produce big changes in tree index series and iterative convergence may not occur. Therefore, in this study we used different methods for some chronologies. In most cases we applied a negative exponential curve in combination with the SF method (N=236 tree-ring chronologies), but in some cases a negative exponential or age-dependent curve without SF was used (N=50 tree ring chronologies) to avoid artifact variation in tree growth probably unrelated to climate. The tree ring chronologies were produced with the RCSigFree and ARSTAN programs (Tree Ring Lab-LDEO, Columbia University).

5. Point by point regression: the drought reconstruction method.

To reconstruct the austral summer (DJF) scPDSI grid from the 286 tree ring chronology network for the SADA domain, we used the well-tested point-by-point Regression method [PPR (10-13)]. This sequential method automatically applies regressive models to the principal components (PC) of the tree ring chronologies during a common calibration period between the predictors (tree rings) and the predictands (scPDSI data) for each grid point of the scPDSI grid (14). The PPR approach uses a search radius around each grid point of the scPDSI grid to locate tree ring chronologies with plausibly stable causal relationships with the grid point in question. This process avoids the need to grid tree ring data and allows each chronology to be separately analyzed as a predictor of scPDSI in the past. There is no *a priori* specific search radius and several considerations need to be made during the selection, such as the geographical distribution of tree ring series, topography, and climatology. For the North American Drought Atlas (NADA) the optimum search radius to reconstruct PDSI was 450 km. However, for the MADA and ANZDA, in which the tree ring networks were more irregularly distributed (mainly in mountain regions), an ensemble of different search radii was used. In South America the tree ring chronologies developed are largely distributed along the Andes Cordillera and large low elevation areas (Patagonian steppe, the Pampas and Chaco region) have no or very short tree ring chronologies, not suitable for inclusion in the database. Larger climate patterns tend to occur over flat areas with relatively low topographic complexity (e.g. the Great Plains in North America or the Mongolian steppes) and climate variability can be captured by tree rings from these or adjacent areas. Each grid point reconstruction was produced using a minimum of 20 tree ring chronologies. However, where insufficient predictors occurred within the initial search radius, the range was progressively expanded by 50 km until the minimum number of chronologies were located. In the Andes region a short radius is more useful to avoid the inclusion of too much noise due to topographic complexity, whereas in flat areas without tree ring chronologies it was necessary to use larger search radii. The reconstructed scPDSI over regions without tree ring chronologies was therefore estimated using predictors mostly from the Andes. Consequently, an ensemble of search radii with distances of 200, 500, 800, 1100, and 1500-km was used, similar to the approach used to develop the MADA (12). Another PPR variable that can be optimized is the screening probability. This variable defines the correlation probability threshold for retaining the best subset of candidates to use for reconstruction, but may also discard useful tree ring predictability information if screening probabilities are too restrictive. Here, we do not use a hard screening threshold, but instead weight all of the tree ring series within a given search radius by the power (p) of their correlations with the grid point scPDSI over the calibration period. We use an ensemble approach with unweighted (p=0) and weighted power correlation (p=1; p=2). Using the five search radii and three power weightings, we created a 15-member ensemble reconstruction, averaging and recalibrating the output model members, and revalidating directly against instrumental data. The average correlation between ensemble members at each grid point were then calculated. This averaging process has been shown previously to reduce noise and increase reconstruction skill (10, 12, 13). The 15-member ensemble mean, based on the bi-weight robust mean, shows a more parsimonious representation of the results and modestly improved accuracy in the model statistics in most cases compared to individual ensemble members.

Due to the modulating effect of the Andes and the influence of distinct oceanic and atmospheric patterns such as the El Niño Southern Oscillation, the Southern Annular Mode, and the South American Summer Monsoon, South America's precipitation regime is particularly variable and different trends in precipitation exist on different sides of the Andes (15), particularly in the high elevation Andes between 24º and 38º S. To avoid predictors in the scPDSI reconstruction from west (east) of the Andes to have influences on a grid point on the east (west) of the Andes, where climate trends could be opposite, we ran two independent ensemble PPR (EPPR). The first PPR omits tree ring chronologies from the Chilean region (west side of the Andes between 24º-38ºS) and considers all remaining tree ring chronologies as predictors. The second PPR only considered predictors from the limited sites west of the Andes. Subsequently both 15-member ensemble reconstructions were merged to create a final reconstruction. This merging process may cause artificial abrupt changes at the borders. To avoid possible constrasting changes, both ensemble reconstructions share the chronologies from the Chilean region located between 20º-24ºS and 38º-41ºS. Since the austral summer (DJF) span two calendar years, we assign to each one of the 600 scPDSI reconstructed summers the calendar year of December. i.e. The summer corresponding to the period 1990-1991 is assigned the year 1990.

6. Calibration and verification statistics of the reconstruction model.

As mentioned in the instrumental data section, we observe a sharp decrease in the number of meteorological stations and limited spatial sampling in the SADA domain before 1951 (Fig. S1). The first reconstruction experiments therefore used the period 1975-2000 for calibration and 1950-1974 for verification. The range of variability represented within this calibration period is strongly influenced by the positive phase of the Pacific Decadal Oscillation (PDO) between the mid-1970s and late 1990s, which had a strong influence on rainfall variability across much of South America.

For the second reconstruction experiments, we calibrated our reconstruction models on the full 1951-2000 period, which is the best represented by instrumental data, and verified on the 1921-1950 period, characterized by fewer stations and poorer spatial representation. For the calibration period we calculate the well-known coefficient of determination (CRSQ or R^2) and the cross-validation reduction of error [CVRE (see Fig. 1b,c from the main text)]. Statistics for the verification period include the square of the coefficient of determination (VRSQ), the reduction of error (VRE), and the coefficient of efficiency (VCE) for the period 1921-1950 (Fig. S4). Details of verification statistics are given in Cook et al. (13, 14). VRSQ is a measure of fractional common variance, and has widespread use in dendroclimatology (14). Figure S4a shows the highest fraction of variance (>40%) over southern Brazil, central Chile and northern Patagonia, where high-quality instrumental data were available during the verification period. The VRE map (Fig. S4b) shows a very similar pattern, while the VCE indicates some reconstruction skill for only about 10% of the SADA domain (Fig. S4c). The VCE is the most rigorous of these verification statistics and the SA areas with poor instrumental and tree ring representations generally do not pass this test.

In summary, these verification statistics based on split calibration/validation methods indicate that the reconstruction models have relatively low predictive power. However, these results may be expected considering the low number of instrumental records over the 1921-1950 verification period. Figure S4d shows the weakest spatial correlation coefficients between instrumental and reconstructed scPDSI indices during 1921-1950 (mean=0.07; median=0.06). However, a sharp increase in spatial correlations was observed for the period 1960-2000 (mean=0.5; median=0.52). Based on the experiments above, calibration/validation of the SADA used a leave-one-out approach (16, 17). We selected the CVRE (see Fig. 1c from the main text) as the target verification stat for the reconstruction models, because the CVRE is based on a leave-one-out procedure. This method is very useful when the observed records are short, allowing the calibration and validation of the model using the full range of scPDSI data from 1951 to 2000. The approach tests the model's ability to predict new data that were excluded from the prediction, in order to flag problems of overfitting or selection bias and to give insight on how the model will adjust to an independent dataset. This technique works by partitioning a sample of a known dataset into complementary subsets, against which the model is tested. To reduce the variability and to give an estimate of the model's predictive performance, it is necessary to perform multiple runs of cross-validation using different partitions, and then average the multiple validation results.

7. Queens Case Imputation and Smoothing (QCIS)

The grid point reconstructions generated by the EPPR method may vary in their temporal length due to the different time periods covered by the chronologies available within each of the five search radii. The number of empty grid points also increases back in time. Additionally, "pixeled noisy" patterns and the presence of occasional "erratics" (e.g., reconstructed values inconsistent with surrounding values) are apparent in the reconstructed fields, which are assumed to be due in part to the strictly local reconstruction properties and random effects of the EPPR reconstruction models. This implies the need to smooth the SADA reconstruction field in a coherent manner. This was done by applying to each grid point reconstruction the Queen's Case Imputation and Smoothing (QCIS) methods, based on the Queen's Case Adjacency model used in spatial statistics (18). This method allows for local re-estimation and smoothing of the annual fields using the following equation:

$$Y_{i,t} = \Sigma \beta_j X_{j,t} \quad j = 1,9 \quad i = 1,N \quad t =1,M,$$

Where *Y* is the smoothed field and *X* is the initial, unsmoothed reconstruction field. Where *N* is the total number of grid points and *M* is the total number of years. The QCIS method uses a 9-point regression kernel to re-estimate the reconstruction at center grid point *i* for each year *t* using the *j* (1-8) surrounding grid points reconstructions produced initially by EPPR, along with the center grid point reconstruction itself at *i.* The addition of grid point *i* as a predictor, guarantees a new centrally weighted estimate at that grid point. The number of *j* grid points is <8 at the borders of the domain or in areas with empty reconstruction grid points. The regression betas (β_j) of the 9 reconstructions determine the relative weighting of the predictors of the center grid point reconstruction. To produce each new QCIS grid point reconstruction, QCIS recalibrates the reconstruction at grid point *i* using the available reconstructions at *i* and *j* as predictors and the same instrumental climate data (predictand) used by EPPR. Similar to EPPR, this procedure is applied point by point over the field. We also used the same calibration and verification periods, and the same principal components regression method used in producing the original EPPR field reconstruction.

The regression kernel locally smooths each spatial field of reconstructions, resulting in a central weighted average of up to 9 prior reconstructions. This smoothing process eliminates "erratic" values. Moreover, the imputation process in empty grid points *i* can occur when adjacent *j* grid points cover a longer time period than *i*, hence the new QCIS reconstruction at grid point *i* will be extended back in time using the EPPR nesting procedure. This imputation and smoothing method can be applied iteratively *k t*imes with progressively more smoothing of the field. For the SADA field we used up to 2 QCIS iterations. Figure S5 shows the effects of imputation and smoothing over four original reconstructed years after the application of the QCIS method. The main wet/drought spatial patterns are preserved after QCIS application for the four years. However, the "pixeled noisy" patterns found in the "Original fields maps" were highly reduced by the smoothing QCIS process (QCIS fields). Additionally, the empty grid points (8%) in the northeast of the domain at year 1400, have been filled by the imputation process. Complete fields in the SADA begin in C.E. 1490.

8. Historical hydroclimate reconstructions.

Historical documents from Bolivia, Chile, and Argentina have allowed the development of continuous high-resolution reconstructions (seasonal, annual) of climatic variations during past centuries (19). In order to validate our drought/pluvial reconstructions with independent records of climate variability, we selected three regions (Fig. 1 of the main text) for which hydroclimatic reconstructions have been developed from historical documents. We compared these independent document-based reconstructions with the three regionally averaged scPDSI time series (Fig. S6). All the historical hydroclimate events and the regional scPDSI averaged records are compiled in Data S1.

Altiplano region: Gioda and Prieto (20) reconstructed the interannual precipitation variability from Potosí, Bolivia, for almost 200 years (1585-1807 period). Silver extraction from the Potosí mine (4000 masl), vital to the Spanish economy at that time, was highly dependent on water runoff used to power the silver mills. The Spanish consistently recorded pluvials and droughts during the spring–summer season. These were compiled in the Actas Capitulares archives of Potosí (20). Data S1 shows dates of the 54 dry and very dry events and the 35 wet and very wet events used for comparison with the averaged scPDSI series for the Altiplano area framed between 17-23ºS latitude and 67-70ºW longitude (Fig. S6a and Fig. 1a main text).

Central Chile region: Historical information of snowy and dry event years was used to reconstruct past hydroclimate variability in the Andes from central Chile and west Mendoza, Argentina, from the 16th century to 1998 (21). The list of dry and snowy events came from the following sources: 1) documentary reports on the state of the snow in the main pass that links Santiago and Mendoza, between 1760 and 1890 (22); 2) newspaper reports of snow depth along the same international pass from 1885 to 1998 (22, 23); 3) reports on discharge of the Mendoza river basin for the period 1600-1960 (24); 4) list of wet years as evidence of El Niño strength between 1535 and 1900 (25). The list of the historical extreme events is reported in Data S1. Figure S6b, shows the comparison and good correspondence between the historical snowy and dry events with the averaged scPDSI for the central Chile region.

La Plata Basin region: Prieto (26) reconstructed the Parana River floods between 1585 and 1815 based on written Spanish records from the cities of Santa Fe and Corrientes. These records are mainly local, often weekly, government reports (the Actas Capitulares), which document socioeconomic and environmental events, especially those with significant economic impacts. Data S1 reports the dates of the 38 floods of the Paraná River between 1585 and 1815 (26) that were used to compare with the scPDSI average for the area between 31-37º S latitude and 56-60º W longitude. Again, good correspondence was found between flood occurrence and positive scPDSI records (Fig. S6c).

9. Changes in extremes in South America regions

Four regions experiencing different climate conditions were selected to explore scPDSI variability and the return time of extreme events: the Altiplano, central Chile, La Plata basin and west Patagonia (Fig. S7). The scPDSI reconstructions for the four regions are characterized by inter-annual to multi-decadal variations. Severe persistent droughts and pluvials were identified in each region (left panels Fig. S7a-d).

The return-time analysis for the Altiplano (Fig. S7e) showed that the frequency of extreme dry events was the highest (1-event/15yrs) in the second half of the 20th century, but was not much different than the 17th and 18th centuries (1-event/18yrs). However, no pluvials occurred during most of the 20th century. The opposite situation took place during 15th century where just one dry extreme event was recorded, while one pluvial occurred every 18 years. The return-time analysis of extreme drought events in central Chile was relatively constant over the study period, ranging between one dry event every 20-30 years (Fig. S7f). Extreme pluvial events show non-stationary frequency occurrences over the study period (Fig. S7f). Low frequencies of extreme pluvial occurrences were recorded during the first half of the 18th and second half of the 20th centuries

(Fig. S7f), while high frequencies were recorded during first half of the 15th (1-event/12-15yrs) and the first half of the 17th and 19th centuries (1-event/17-19 yrs). The region of La Plata basin is characterized by a sustained increase in the rate of occurrence of pluvial extremes, with the highest rates recorded during the last decades of the 20th century (1-event/12 yrs; Fig. S7g), while the return time of extreme drought events was high during the 16th and 17th centuries (1-event/13-20 yrs) and maintained relatively low and constant activity during the 18th, 19th, and 20th centuries (1-event/20-30 yrs; Fig. S7g). The Patagonia region showed reduce occurrence of extreme drought events during the 15th and 16th centuries, and increased since the mid-17th to the end of the 20th century (1-event/17-19 yrs; Fig. S7h). Extreme pluvials were more variable and show low return periods during the 15th, second half of the 18th, and first half of the 19th centuries, and were highest during the second half of the 20th century (1-event/12 yrs; Fig. S7h).

10. Large-scale ocean-atmosphere climate datasets (SST, SST_N3.4, GPH500 and SAM)

We retrieved the global dataset of monthly averaged SST fields from the Hadley Centre Sea Ice and SST (HadISST) dataset that is available online from the National Center for Atmospheric Research (NCAR, 27). The HadISST data record extends back to 1870, and is spatially gridded with 1ºx1º resolution, ranging in longitude from 180°W to 180°E. We also downloaded monthly anomalies of the HadISST averaged over the tropical Pacific NINO 3.4 region, an area between 170º-120ºW longitude and 5ºN-5ºS latitude. This dataset is available online from the Royal Netherlands Meteorological Institute (KNMI, 28)

The global dataset of monthly averaged geopotential height at 500 mb (GPH500) was retrieved from the National Center for Environmental Prediction (NCEP, 29). These data cover the period 1948–present and have a spatial resolution of 2.5ºx2.5º. Finally, the Southern Anular Mode index (SAM; 1957-present) was downloaded from the British Antarctic Survey (BAS, 30) and the methodology of the index development is discussed in detail in Marshall (31).

11. Maximum Covariance Analysis for instrumental scPDSI and climate drivers

To check the robustness of the Maximum Covariance Analysis (MCA) results derived from the reconstructed scPDSI from the SADA and ANZDA, we applied the MCA to the instrumental scPDSI and summer (DJF) Sea Surface Temperatures (SSTs) and the summer (DJF) Geopotential Heights at 500 hpa (GPH500). Figure S8 maps the MCA patterns for the latter and indicates that there is a strong degree of similarity between the spatial patterns of the coupled variability derived from MCA using the instrumental and reconstructed scPDSI in the analysis.

12. Comparisons to other ENSO and SAM reconstructions

The ENSO and SAM estimation (ENSO-e and SAM-e), derived from the MCA (Fig. 4c,d), were compared with other ENSO and SAM reconstructions (Fig. S9). Tree-ring based NINO 3.4 index reconstructions were developed by Cook et al. (32), Li et al. (33) and Cook et al. (34), while multiproxy NINO 3.4 index reconstructions were developed by Wilson et al. (35) and Emile-Geay (36). Figure S9, demonstrates positive correlations between ENSO-e and the five reconstructions, ranging from 0.20 (vs. Wilson 2010) to 0.73 (vs. Cook 2018). The 30-yr moving correlation, plotted below each comparison (Fig. S9), shows changes in the stability of the relationship across the entire 500 yrs, with some periods very strong ($r > 0.6$) and others weak ($r < 0.1$).

SAM reconstructions are few in relation to those of ENSO, and they are not totally independent since they share tree ring proxies. Here we compare our estimated SAM-e with one tree ring (37) and two multi-proxy based SAM reconstructions (38, 39). Figure S10 show the comparisons and moving correlations between these records. SAM-e is well correlated with the Villalba and Datwyler reconstructions (r=0.45 and r=0.52, respectively), while it is weakly correlated with the Abram et al. reconstruction. The moving correlations below each reconstruction comparisons are relatively stable over time for the two first comparisons, and is weak and unstable for the last reconstruction.

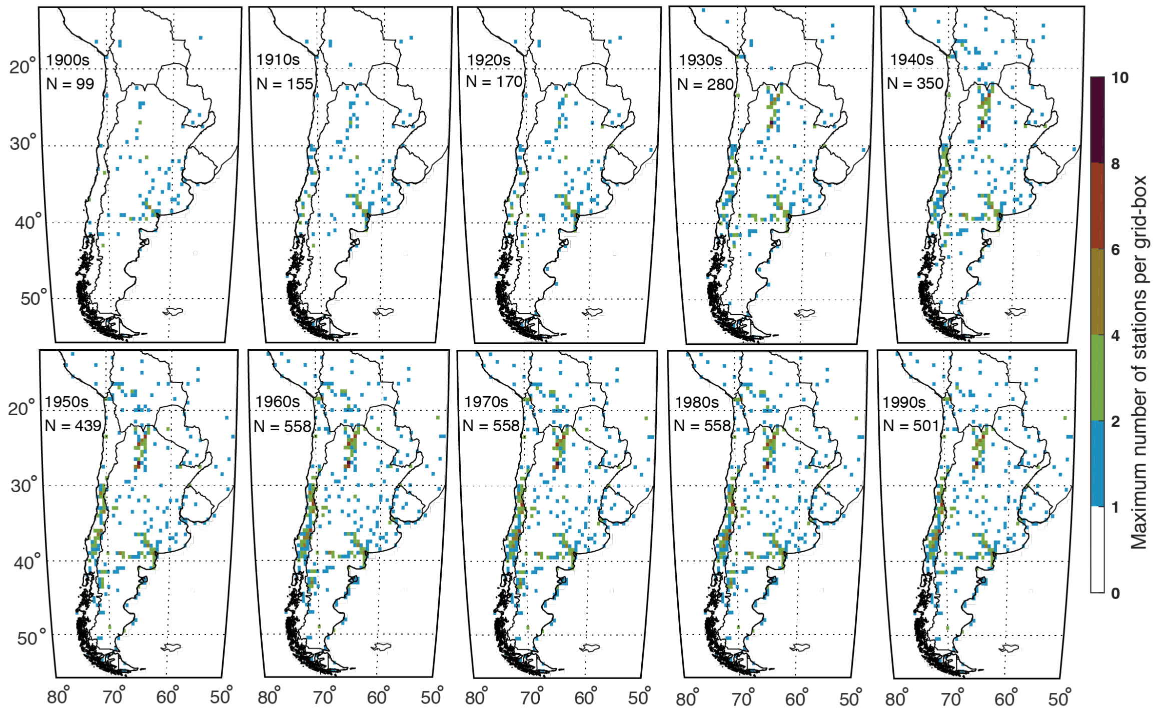

Fig. S1. Spatial distribution and number of available precipitation stations by decade for interpolation on the half-degree regular grid used to produce the CRU TS precipitation field. A relatively good spatial representation of stations over the SADA domain is observed since the 1950s.

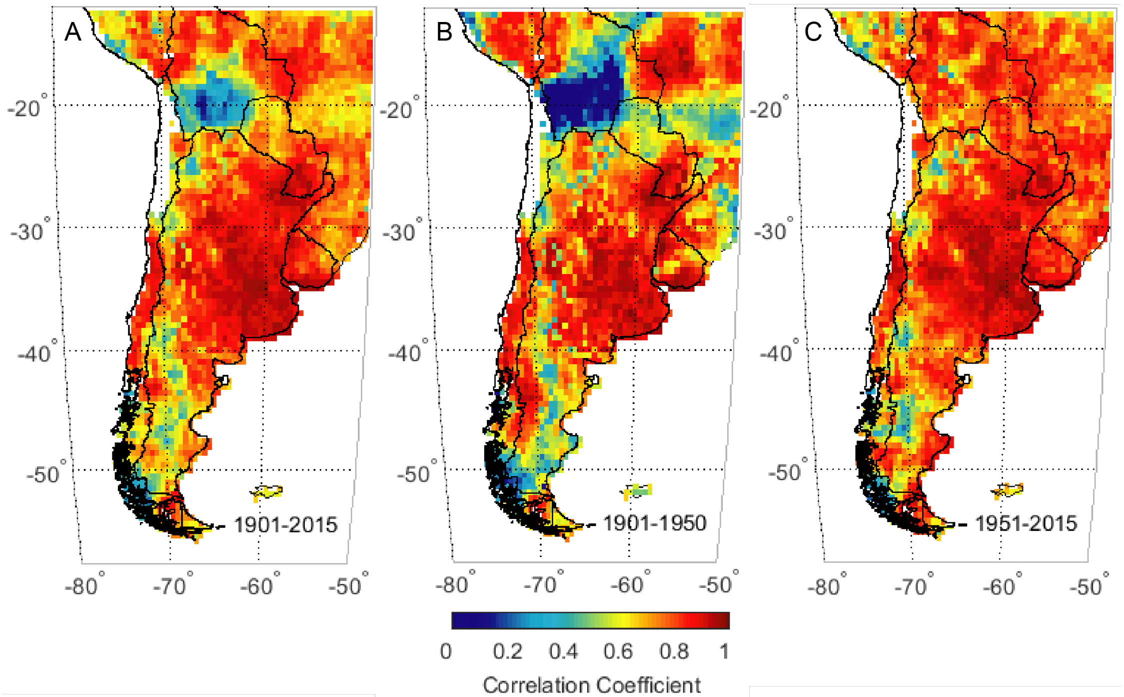

Fig. S2. Field correlation coefficients between CRU-TS 3.24 DJF average precipitation dataset and the DJF average of the ensemble precipitation dataset used in this study for the periods (A) 1901-2015, (B) 1901-1950 and (C) 1951-2015.

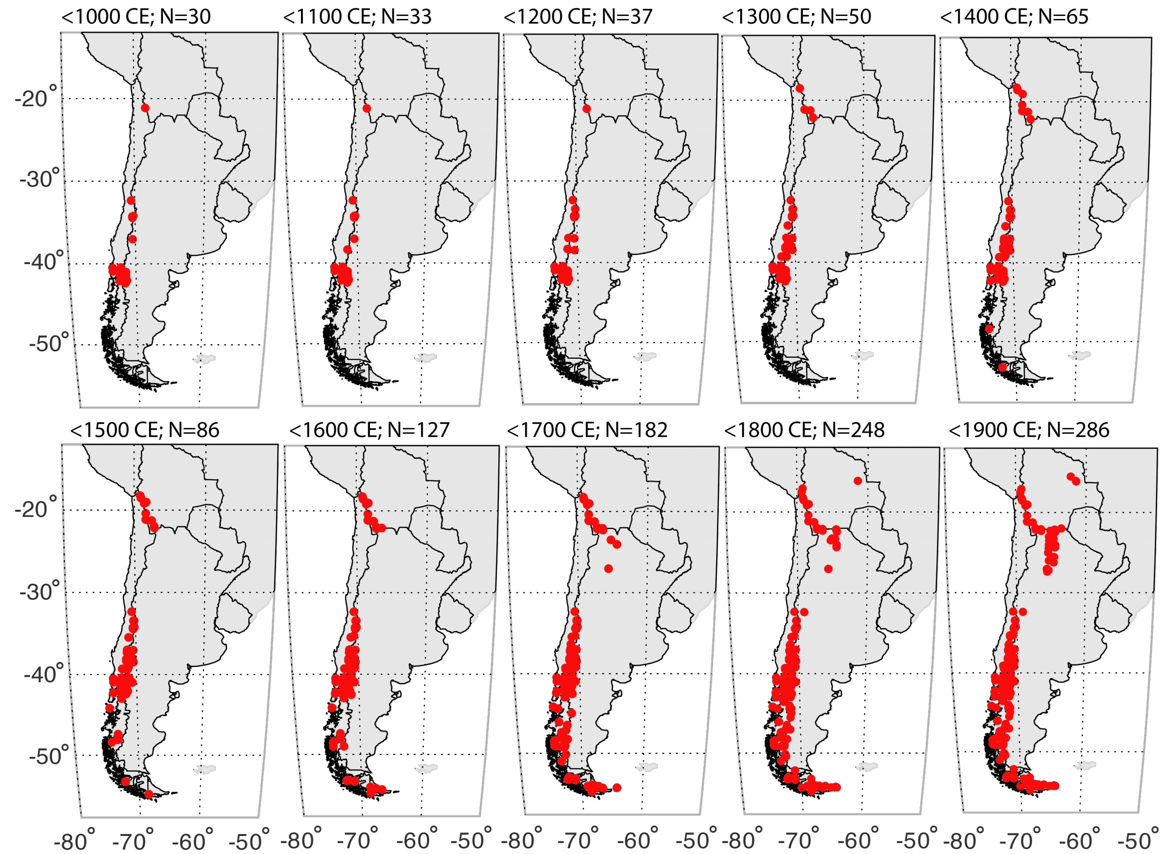

Fig. S3. Geographical distribution of tree-ring chronologies in the SA study domain during the last millennium. The N located in the top of each box represents the number of tree ring chronologies used to reconstruct the scPDSI. Note the significant reduction in tree ring chronologies before 1400 C.E.

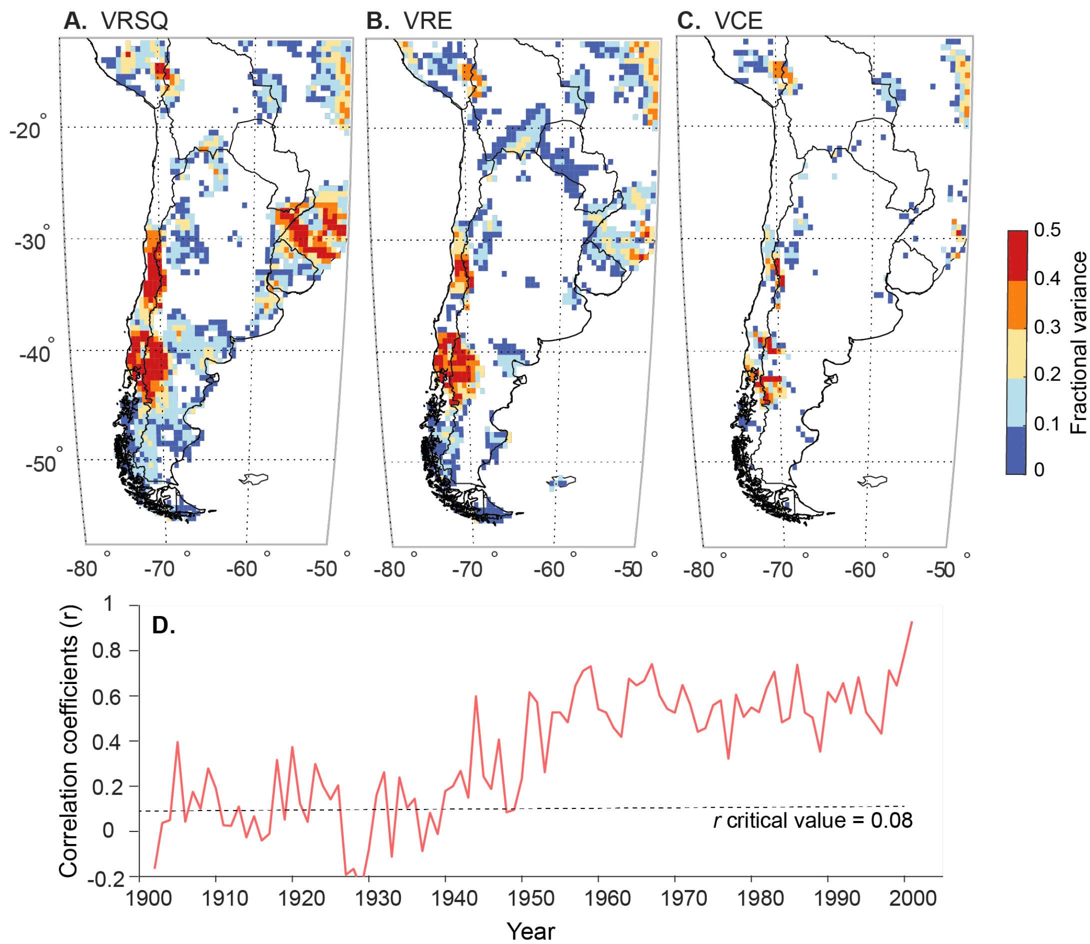

Fig. S4. Validation statistic maps of the 15-member ensemble-average SADA reconstructions for the period 1921-1950. All statistics are in units of fractional variance. Only those grid points that verify at the 1-tail 90% confidence level for (A) VRSQ, and include (B) VRE and (C) VCE values >0, are plotted. (D) Time varying series of the spatial correlations between the instrumental and reconstructed scPDSI index for the period 1901-2000. Note the small correlation coefficients between 1901-1950 and the increase in the spatial correlations beginning in the 1950s.

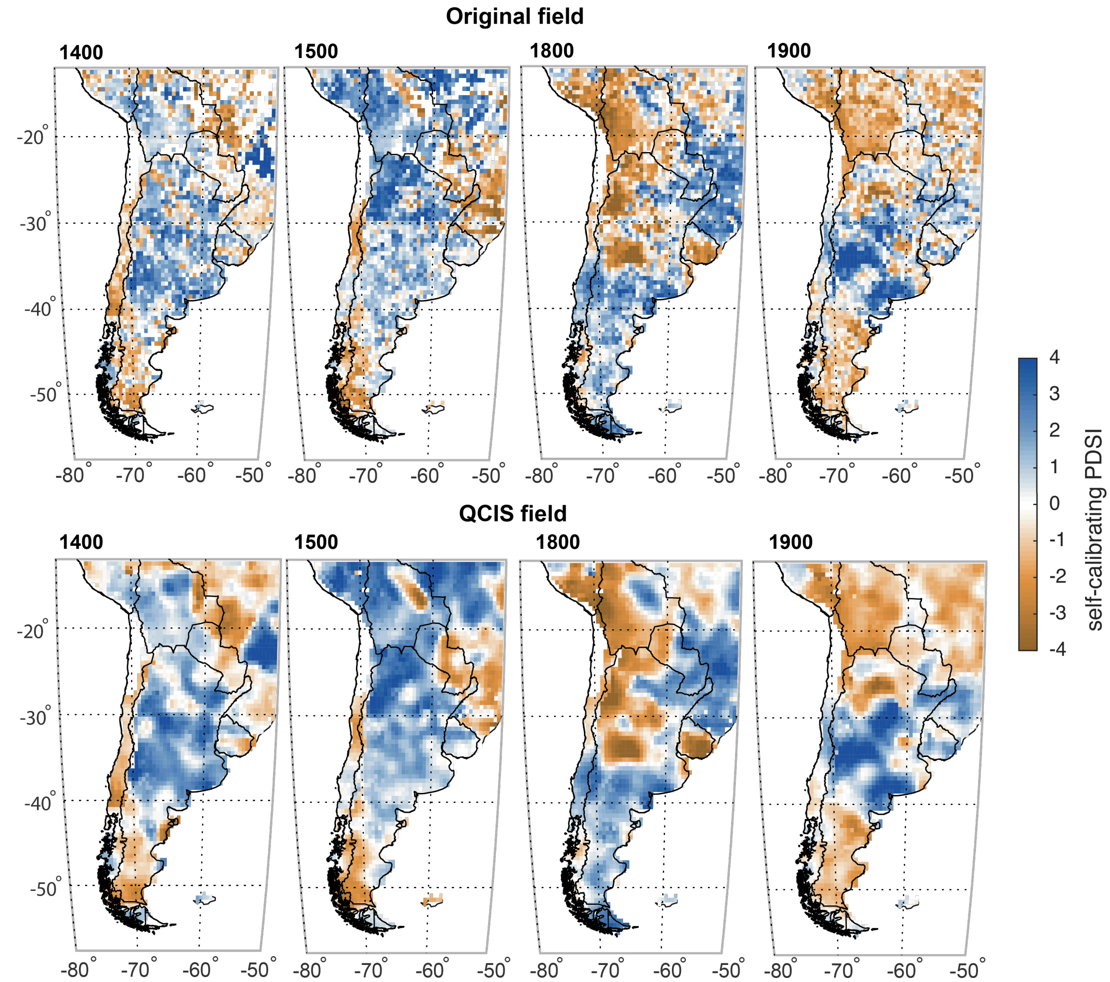

Fig. S5. Comparisons of four annual SADA maps (1400, 1500, 1800 and 1900) showing the effects before (Original field) and after (QCIS field) the application of the QCIS method on the EPPR reconstructed fields.

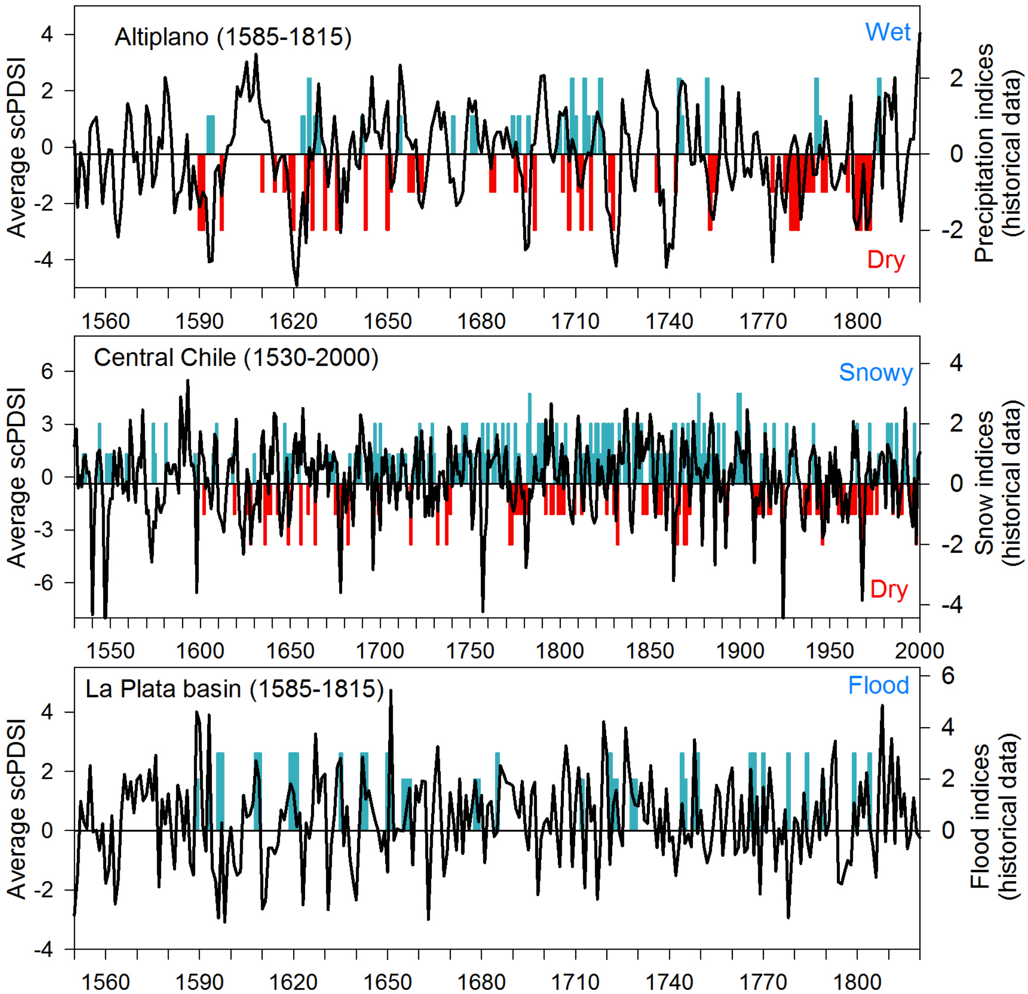

Fig. S6. Comparison between historical hydroclimate (blue and red bars) and tree ring based scPDSI reconstructions (solid black line) for (A) Altiplano, (B) Central Chile and (C) part of the La Plata basin. Historical data and the tree ring reconstructions show correspondence during wet and dry years.

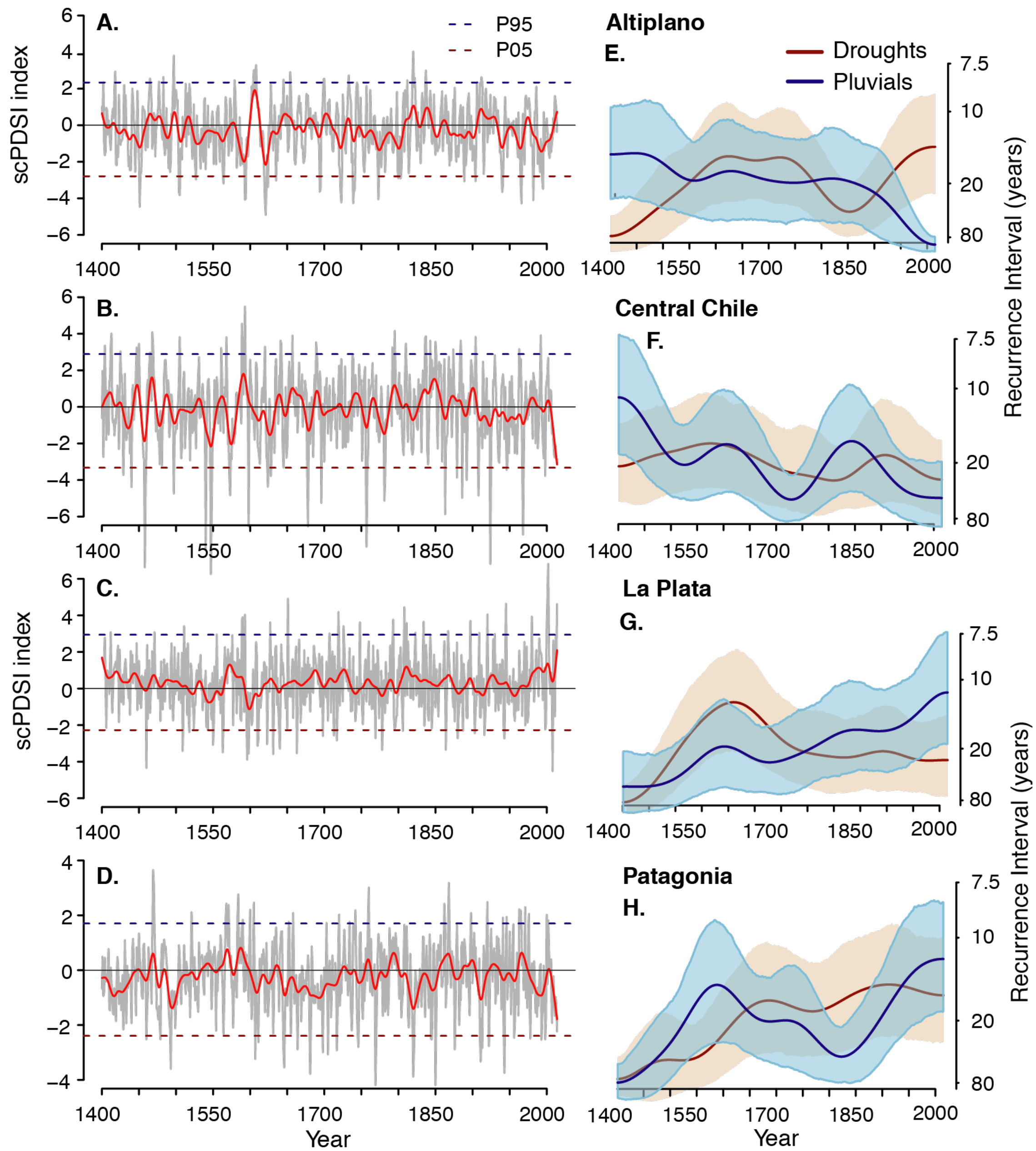

Fig. S7. Austral summer (December-January-February) scPDSI reconstruction average for four regions: (A) Altiplano, (B) central Chile, (C) la Plata basin and (D) Patagonia, for the period AD 1400–2000. The 25-year smoothing-spline curve (red line) highlights the multi-decadal variability. Red and blue short dashed lines indicate the 5% and 95% percentiles, respectively, from which extreme dry/wet events were selected for the return-time analysis in panels E to H. (E-H) Time-varying frequency of the occurrence rate of extreme dry/wet scPDSI events, between 1400 and 2000. A kernel smoothing method was used with a bandwidth of 50 years. The shaded areas (blue and orange) represent 95% confidence intervals based on 1000 bootstrap simulations.

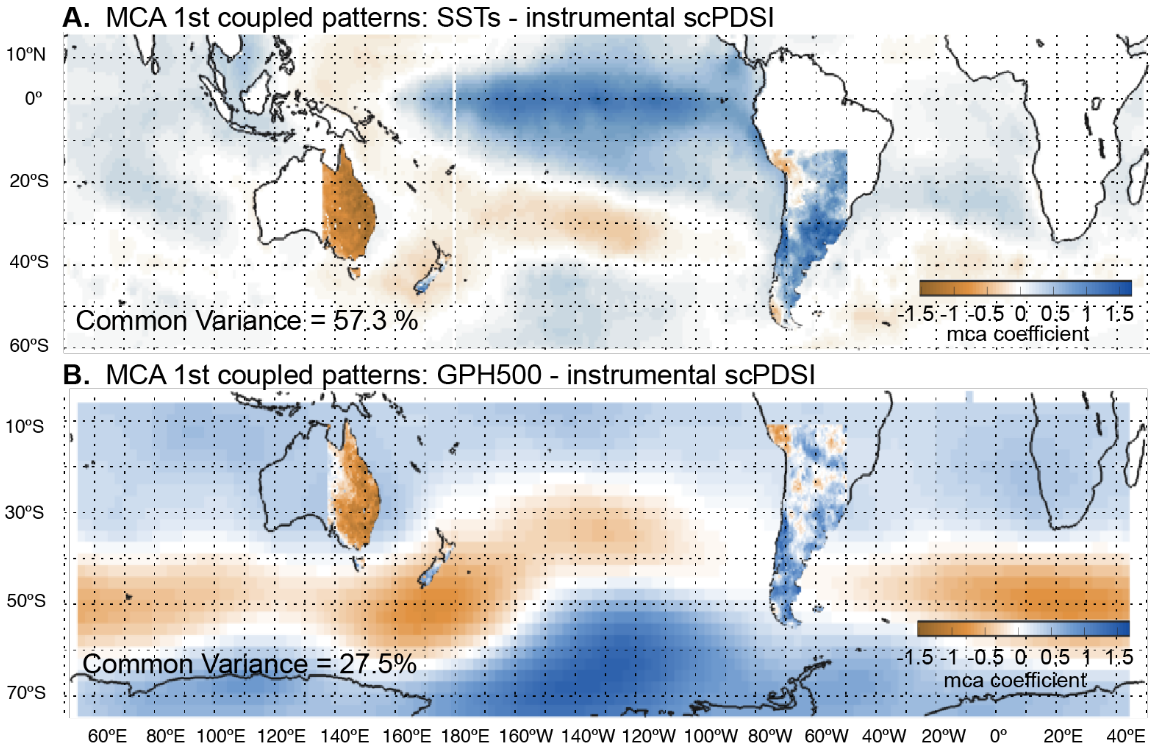

Fig. S8. Coupled spatiotemporal patterns of variability between large-scale ocean-atmosphere climate forcing and instrumental scPDSI fields from the same domain as SADA and ANZDA. Spatial patterns of the main leading Maximum Covariance Analysis (MCA) mode between instrumental scPDSI and (A) austral summer Sea Surface Temperatures over the common period 1901-2015, and (B) austral summer Geopotential Height (500hpa) over the common period 1948-2015.

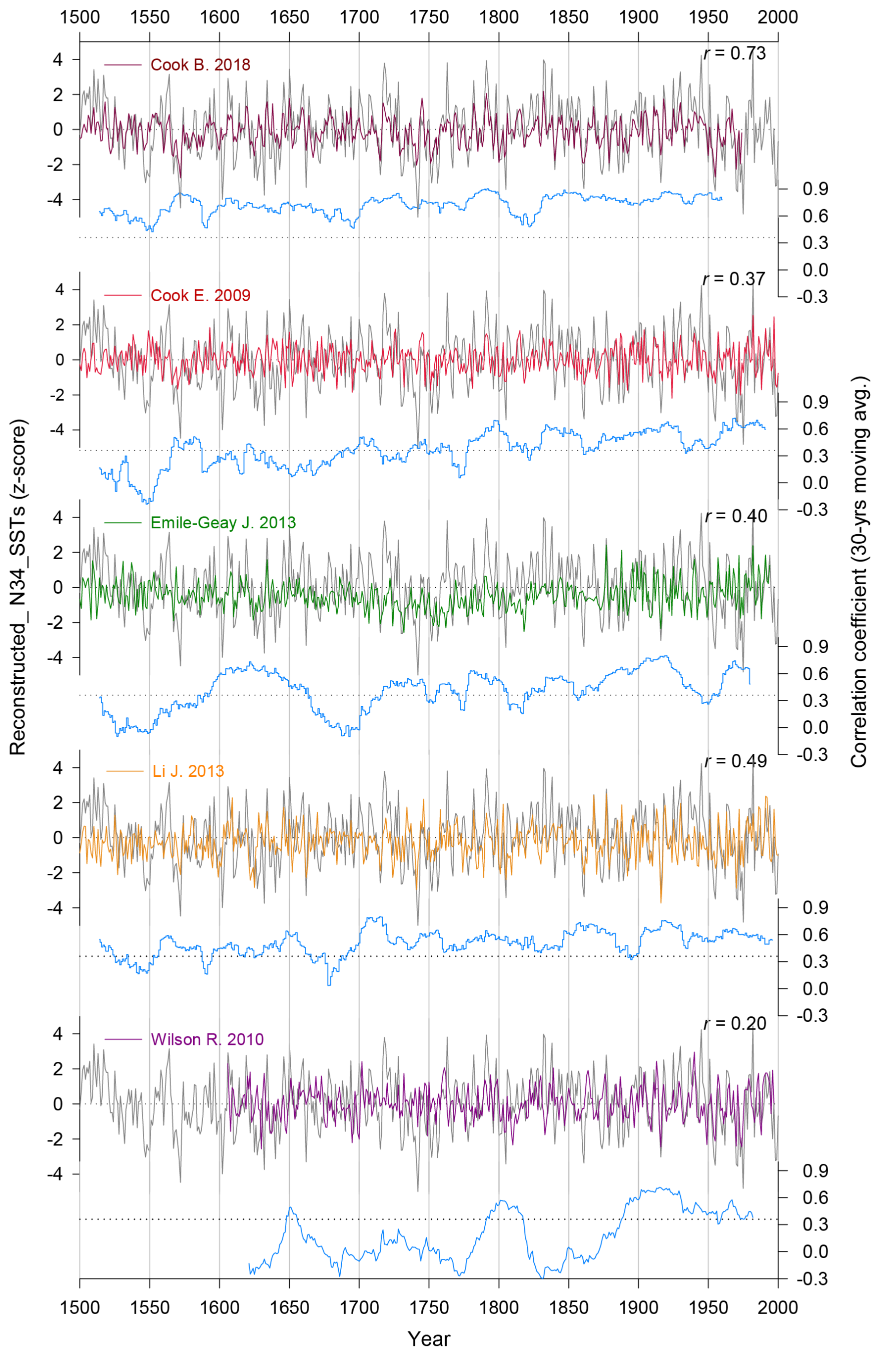

Fig. S9. Comparisons between reconstructed ENSO indices derived from drought atlases (SADA and ANZDA; this study) and other authors during the period 1500-2000 C.E. The estimated ENSO index from the Maximum Covariance Analysis (1st covariance scPDSI pattern) is shown in each panel by the gray line, and the other reconstructions are colored. Correlation coefficients are indicated in the top right of each panel. The blue lines below each pair of ENSO reconstructions represents their 30-year moving correlation. The dotted line represent the 95% confidence level.

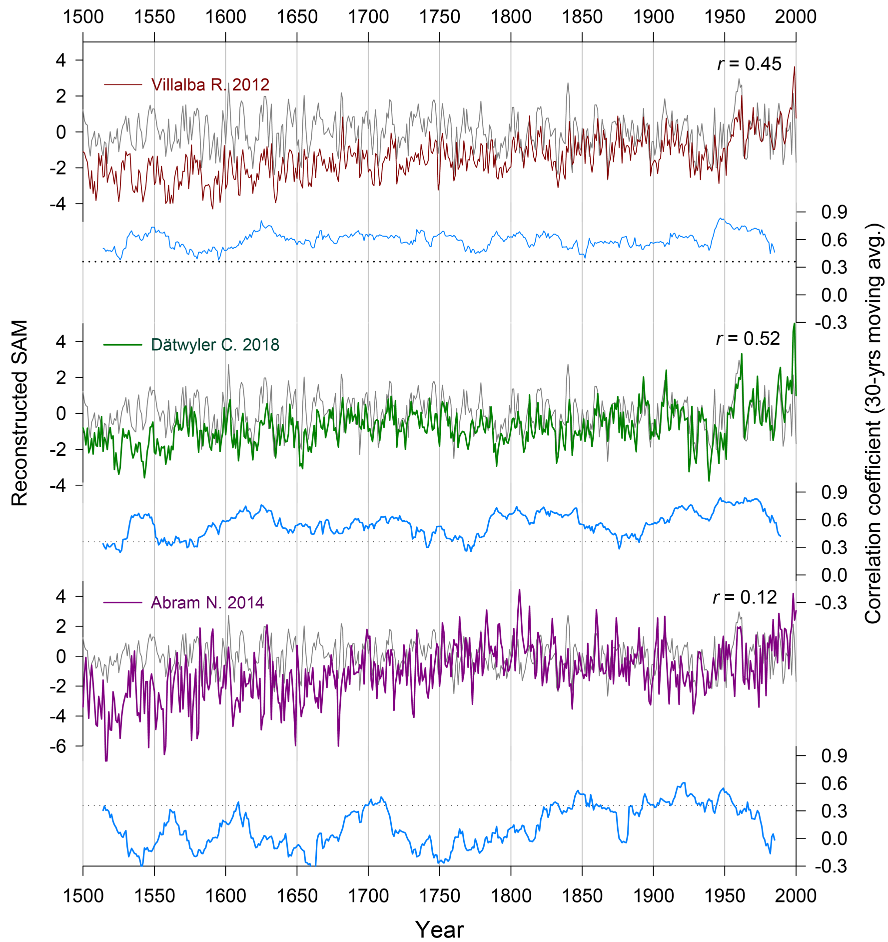

Fig. S10. Comparisons of the SAM indices derived from the drought atlases (SADA and ANZDA; this study) and other authors during the period 1500-2000 C.E. The estimated SAM index from the Maximum Covariance Analysis (1st covariance scPDSI pattern) is shown in each panel by the gray line, and the other reconstructions are colored. Correlation coefficients are indicated in the top right of the panels. The blue line below SAM the reconstructions represents the 30-year moving correlation. The dotted line represent the 95% confidence level.

Table S1. List of tree-ring chronologies used to produce the SADA.

Species	Species Code	Start Year	End Year	Latitude ºS	Longitude ºW	Site Name
Adesmia horrida	ADHO	1768	1986	-32 43	-69 05	MANANTIA
Araucaria araucana	ARAR	1400	2000	-37 38	-71 28	Alul
Araucaria araucana	ARAR	1429	2000	-38 48	-71 12	Batea Mahuida
Araucaria araucana	ARAR	1400	2000	-38 66	-71 70	Captren+Lonquimay
Araucaria araucana	ARAR	1444	1974	-37 51	-71 02	Caviahue
Araucaria araucana	ARAR	1550	2000	-37 52	-71 04	CAVIAHUE
Araucaria araucana	ARAR	1400	2000	-39 27	-71 51	Challupen
Araucaria araucana	ARAR	1400	1974	-38 06	-70 51	Chenque Pehuen
Araucaria araucana	ARAR	1675	2000	-38 25	-71 36	Coloradito
Araucaria araucana	ARAR	1607	2000	-38 25	-71 33	Colorado Lara
Araucaria araucana	ARAR	1640	1974	-37 48	-71 04	Copahue
Araucaria araucana	ARAR	1525	2000	-39 33	-71 02	Ea Nahuel Mapi
Araucaria araucana	ARAR	1512	2000	-38 81	-71 27	Icalma
Araucaria araucana	ARAR	1617	1976	-39 36	-71 22	Lago Tromen
Araucaria araucana	ARAR	1400	2000	-39 37	-71 26	Lanin
Araucaria araucana	ARAR	1400	1974	-38 59	-71 03	Lonco Luan
Araucaria araucana	ARAR	1400	2000	-38 25	-71 36	Nalca+ColoradoChile
Araucaria araucana	ARAR	1676	2000	-39 09	-71 15	Norquinco2
Araucaria araucana	ARAR	1400	2000	-38 50	-71 05	Paso del Arco
Araucaria araucana	ARAR	1400	1983	-39 37	-71 25	Paso Tromen
Araucaria araucana	ARAR	1400	2000	-37 50	-71 02	Piedra del Aguila
Araucaria araucana	ARAR	1606	2000	-39 19	-71 17	Pinalada Redonda
Araucaria araucana	ARAR	1424	2000	-38 38	-70 45	Pino Hachado
Araucaria araucana	ARAR	1400	1974	-38 53	-70 37	Primeros Pinos
Araucaria araucana	ARAR	1589	1989	-39 08	-71 11	Pulmari
Araucaria araucana	ARAR	1459	2000	-39 28	-71 46	Quetrupillan
Araucaria araucana	ARAR	1591	2000	-39 24	-70 48	Rahue
Araucaria araucana	ARAR	1592	2000	-37 56	-71 22	Ralco
Araucaria araucana	ARAR	1450	2000	-39 06	-71 19	Remeco
Araucaria araucana	ARAR	1400	2000	-39 13	-71 10	Rucachoroi2
Araucaria araucana	ARAR	1400	2000	-38 18	-71 42	Tolhuaca
Araucaria araucana	ARAR	1673	2000	-37 58	-71 18	Vizcacha
Austrocedrus chilensis	AUCH	1733	1975	-37 21	-71 36	Abanico
Austrocedrus chilensis	AUCH	1823	1975	-34 55	-70 42	Alto de las mesas
Austrocedrus chilensis	AUCH	1589	1991	-40 42	-71 16	Arroyo minero
Austrocedrus chilensis	AUCH	1400	2000	-34 29	-70 14	Blanco
Austrocedrus chilensis	AUCH	1400	2000	-34 26	-70 19	Ciprecillos
Austrocedrus chilensis	AUCH	1473	2000	-34 20	-70 17	Ciprecito
Austrocedrus chilensis	AUCH	1576	2000	-40 30	-71 09	Co Catillo
Austrocedrus chilensis	AUCH	1596	1989	-39 56	-71 08	Collunco alto
Austrocedrus chilensis	AUCH	1723	1989	-40 42	-71 09	Confluencia 2
Austrocedrus chilensis	AUCH	1543	2000	-40 43	-71 08	Cuyin Manzano
Austrocedrus chilensis	AUCH	1461	1989	-40 44	-71 06	Dedo de dios
Austrocedrus chilensis	AUCH	1400	2000	-32 39	-70 49	El Asiento
Austrocedrus chilensis	AUCH	1400	2000	-34 48	-70 29	El Azufre
Austrocedrus chilensis	AUCH	1400	2000	-34 29	-70 26	El Baule+Agua de la Muerte
Austrocedrus chilensis	AUCH	1489	2000	-40 44	-71 06	El Centinela
Austrocedrus chilensis	AUCH	1400	2000	-34 32	-70 34	El Cepillo
Austrocedrus chilensis	AUCH	1641	1975	-37 21	-71 30	El Chacay
Austrocedrus chilensis	AUCH	1497	2000	-41 02	-70 59	El Guanaco
Austrocedrus chilensis	AUCH	1690	1974	-41 59	-71 15	El Maiten
Austrocedrus chilensis	AUCH	1484	2000	-40 39	-71 24	El Mirador
Austrocedrus chilensis	AUCH	1553	2000	-35 36	-70 54	El Venado
Austrocedrus chilensis	AUCH	1540	2000	-42 57	-71 13	Estancia Teresa
Austrocedrus chilensis	AUCH	1400	2000	-37 08	-70 36	Huingango New
Austrocedrus chilensis	AUCH	1690	2000	-41 04	-71 59	La Fragua
Austrocedrus chilensis	AUCH	1508	2000	-40 03	-71 17	La Hormiga
Austrocedrus chilensis	AUCH	1700	1974	-43 01	-71 34	Lago Terraplen
Austrocedrus chilensis	AUCH	1700	2000	-37 20	-71 32	Laja

Austrocedrus chilensis	AUCH	1539	2000	-41 05	-71 09	Los Leones (Cerro Los Leones)
Austrocedrus chilensis	AUCH	1645	2000	-36 42	-71 16	Los Mayos
Austrocedrus chilensis	AUCH	1508	2000	-40 04	-71 02	Los Pinos
Austrocedrus chilensis	AUCH	1400	2000	-34 23	-70 19	Matancilla
Austrocedrus chilensis	AUCH	1400	2000	-35 52	-71 00	Melado+Rancho Maule
Austrocedrus chilensis	AUCH	1567	2000	-42 58	-71 13	Nahuel Pan
Austrocedrus chilensis	AUCH	1400	2000	-37 42	-71 18	Nitrao
Austrocedrus chilensis	AUCH	1562	2000	-39 07	-71 07	Norquinco
Austrocedrus chilensis	AUCH	1741	1991	-41 32	-71 29	Pampa del Toro
Austrocedrus chilensis	AUCH	1679	1991	-40 42	-71 07	Paso del viento
Austrocedrus chilensis	AUCH	1733	1991	-41 11	-70 45	Pilcaniyeu
Austrocedrus chilensis	AUCH	1400	2000	-37 04	-71 25	Polcura
Austrocedrus chilensis	AUCH	1400	2000	-34 48	-70 33	Quebrada los Helados
Austrocedrus chilensis	AUCH	1676	1989	-39 17	-71 16	Quillen
Austrocedrus chilensis	AUCH	1585	2000	-38 04	-71 19	Ralco-Lepoy
Austrocedrus chilensis	AUCH	1400	2000	-34 48	-70 31	Rancho Fonola
Austrocedrus chilensis	AUCH	1572	2000	-39 15	-71 10	Rucachoroi
Austrocedrus chilensis	AUCH	1400	1996	-33 47	-70 15	San Gabriel
Austrocedrus chilensis	AUCH	1650	1991	-41 03	-70 59	San Ramon
Austrocedrus chilensis	AUCH	1613	1975	-34 47	-70 45	Santa Isabel
Austrocedrus chilensis	AUCH	1400	2000	-34 27	-70 25	Uriola este
Austrocedrus chilensis	AUCH	1500	2000	-34 27	-70 26	Uriola Oeste
Cedrela angustifolia	CEAN	1810	1981	-24 36	-64 35	Finca el Rey
Cedrela angustifolia	CEAN	1851	1981	-24 65	-65 25	Rio Blanco
Cedrela angustifolia	CEAN	1729	1982	-27 08	-65 51	Rio Horqueta
Centrolobium michrocaete	CEMI	1836	2000	-16 13	-61 39	Inpa
Centrolobium michrocaete	CEMI	1924	2000	-15 38	-62 24	Palestina
Centrolobium michrocaete	CEMI	1798	2000	-16 19	-61 36	Purupi
Centrolobium michrocaete	CEMI	1847	2000	-15 58	-62 13	Santa Monica
Fitzroya cupressoides	FICU	1400	2000	-41 30	-72 30	Alerce Andino
Fitzroya cupressoides	FICU	1400	1993	-42 16	-72 46	Ayacara
Fitzroya cupressoides	FICU	1400	2000	-41 24	-72 18	Cerro Nevado
Fitzroya cupressoides	FICU	1400	1993	-41 06	-71 46	Horqueta inferior
Fitzroya cupressoides	FICU	1400	1993	-41 50	-71 47	Horqueta Superior
Fitzroya cupressoides	FICU	1400	1995	-41 15	-71 54	La Esperanza
Fitzroya cupressoides	FICU	1400	1993	-41 57	-72 17	Lago Inexplorado
Fitzroya cupressoides	FICU	1400	2000	-41 33	-72 36	Lenca
Fitzroya cupressoides	FICU	1400	1993	-40 50	-72 20	Los Quetro
Fitzroya cupressoides	FICU	1400	2000	-41 36	-72 33	Oro verde
Fitzroya cupressoides	FICU	1400	1996	-40 54	-73 45	Pabilos
Fitzroya cupressoides	FICU	1400	1994	-41 52	-72 32	Patamay
Fitzroya cupressoides	FICU	1400	1992	-41 00	-73 43	Pelada
Fitzroya cupressoides	FICU	1400	1992	-42 44	-71 58	Puerto Cafe
Fitzroya cupressoides	FICU	1400	1995	-40 55	-72 21	Puntiagudo
Fitzroya cupressoides	FICU	1400	1993	-42 35	-71 57	Rio Alejandro
Fitzroya cupressoides	FICU	1400	1991	-41 10	-71 47	Rio Alerce
Fitzroya cupressoides	FICU	1400	1974	-42 09	-71 33	Rio Cisne
Fitzroya cupressoides	FICU	1400	1991	-41 06	-71 48	Rio Frias
Fitzroya cupressoides	FICU	1400	1993	-42 08	-71 50	Rio Motoco
Fitzroya cupressoides	FICU	1400	1987	-42 30	-73 50	Tiuchue Chiloe
Fitzroya cupressoides	FICU	1400	1994	-41 03	-72 38	Volcan Apagado
Fitzroya cupressoides	FICU	1400	1994	-41 10	-72 30	Volcan Osorno
Juglans australis	JGAU	1895	2000	-23 33	-65 01	Arroyo San Lucas
Juglans australis	JGAU	1791	2000	-24 40	-64 35	Cascada Lobitos
Juglans australis	JGAU	1805	1999	-22 04	-63 45	Cauzuti
Juglans australis	JGAU	1740	2000	-24 45	-64 39	Cerro Chanar
Juglans australis	JGAU	1800	2000	-27 40	-65 46	Dique Escaba
Juglans australis	JGAU	1813	1985	-27 42	-65 47	Dique Escaba juo25m
Juglans australis	JGAU	1765	1985	-21 43	-64 24	El Arrayal
Juglans australis	JGAU	1840	2000	-26 27	-64 54	El Cajon
Juglans australis	JGAU	1678	2000	-24 11	-64 32	El Piquete
Juglans australis	JGAU	1858	1981	-26 05	-65 23	Finca las Pichanas
Juglans australis	JGAU	1709	1999	-22 19	-64 38	La Mesada
Juglans australis	JGAU	1826	1979	-25 07	-65 33	Los Laureles

Juglans australis	JGAU	1814	1994	-22 19	-64 40	Los Toldos
Juglans australis	JGAU	1883	2000	-23 34	-64 59	Molular
Juglans australis	JGAU	1779	2000	-23 35	-64 55	Nogalar
Juglans australis	JGAU	1796	2000	-23 32	-65 01	Pampichuela
Juglans australis	JGAU	1883	2000	-24 38	-64 33	Popayan
Juglans australis	JGAU	1688	1998	-23 55	-65 18	Rio Bolsas
Juglans australis	JGAU	1783	1982	-27 08	-65 51	Rio Horqueta
Juglans australis	JGAU	1646	1994	-27 10	-65 53	Rio Horqueta N1
Juglans australis	JGAU	1849	1981	-24 36	-64 35	Rio La Sala
Juglans australis	JGAU	1826	1979	-26 26	-64 57	Rio Nio
Juglans australis	JGAU	1739	1999	-22 49	-64 30	Rio Pescado
Juglans australis	JGAU	1742	1999	-22 20	-64 42	San Jose
Juglans australis	JGAU	1820	1982	-24 36	-64 35	Senda el Ciervo
Juglans australis	JGAU	1872	2000	-25 59	-64 48	Tunillas
Juglans australis	JGAU	1841	1999	-22 21	-64 42	Vallecito
Juglans australis	JGAU	1889	2000	-24 10	-65 23	Yala
Juglans australis	JGAU	1889	2000	-24 13	-65 08	Zapla
Nothofagus betuloides	NOBE	1715	1986	-54 42	-64 40	Bahia Crossley Isla Estados
Nothofagus betuloides	NOBE	1751	1986	-54 50	-65 12	Bahia del Buen Suceso
Nothofagus betuloides	NOBE	1647	1986	-54 50	-64 20	Bahia York
Nothofagus betuloides	NOBE	1729	2000	-44 07	-71 53	Guerrero Rio Los Nevados
Nothofagus betuloides	NOBE	1704	2000	-53 44	-72 28	Isla Santa Ines
Nothofagus betuloides	NOBE	1660	2000	-54 13	-68 28	Lago Despreciado
Nothofagus betuloides	NOBE	1527	2000	-54 22	-68 46	Lago despreciado L.N.
Nothofagus betuloides	NOBE	1577	2000	-54 28	-68 41	Lago Fagnano betuloides
Nothofagus betuloides	NOBE	1489	2000	-55 00	-68 41	Lago Robalo
Nothofagus betuloides	NOBE	1850	2000	-48 24	-73 50	Ofhidro Costa PNBO
Nothofagus betuloides	NOBE	1624	2000	-54 20	-68 49	P.L. Despreciado
Nothofagus betuloides	NOBE	1726	1986	-54 50	-64 22	Puerto Parry
Nothofagus betuloides	NOBE	1528	1986	-54 54	-66 55	Rio Moat
Nothofagus betuloides	NOBE	1702	2000	-44 44	-71 56	Santa Teresa
Nothofagus pumilio	NOPU	1810	2000	-35 35	-70 59	Altos de Lircay
Nothofagus pumilio	NOPU	1666	1986	-54 31	-67 25	Aserradero Isla Grande
Nothofagus pumilio	NOPU	1755	1988	-45 55	-71 45	Balmaceda
Nothofagus pumilio	NOPU	1706	1988	-50 22	-72 47	Buenos Aires Sta cruz
Nothofagus pumilio	NOPU	1741	2000	-50 21	-72 47	Calafate
Nothofagus pumilio	NOPU	1772	2000	-37 55	-71 22	Callaqui
Nothofagus pumilio	NOPU	1816	1996	-50 57	-72 53	Campo Chileno
Nothofagus pumilio	NOPU	1774	1996	-50 57	-72 54	Campo Torres
Nothofagus pumilio	NOPU	1808	1996	-54 16	-68 41	Campo XX Inferior
Nothofagus pumilio	NOPU	1805	1996	-54 17	-68 41	Campo XX Krummholz
Nothofagus pumilio	NOPU	1784	1996	-54 17	-68 41	Campo XX Medio
Nothofagus pumilio	NOPU	1626	1982	-41 15	-71 45	Castano Overo
Nothofagus pumilio	NOPU	1861	1991	-41 09	-71 48	Castano overo1
Nothofagus pumilio	NOPU	1808	1991	-41 09	-71 48	Castano overo3
Nothofagus pumilio	NOPU	1820	1991	-41 09	-71 48	Castano overo4
Nothofagus pumilio	NOPU	1820	1991	-41 09	-71 48	Castano overo5
Nothofagus pumilio	NOPU	1539	1991	-41 09	-71 48	Castano overo6
Nothofagus pumilio	NOPU	1562	1991	-41 09	-71 48	Castano overo7
Nothofagus pumilio	NOPU	1572	1991	-41 09	-71 48	Castano overo8
Nothofagus pumilio	NOPU	1635	2000	-49 18	-73 00	Cerro 30 Aniversario
Nothofagus pumilio	NOPU	1661	1996	-54 14	-68 40	Cerro Balseiro
Nothofagus pumilio	NOPU	1734	1974	-50 25	-72 45	Cerro Buenos Aires
Nothofagus pumilio	NOPU	1730	1996	-51 09	-73 18	Cerro Ferrier A
Nothofagus pumilio	NOPU	1685	1996	-51 09	-73 17	Cerro Ferrier B
Nothofagus pumilio	NOPU	1800	1996	-53 55	-69 43	Cerro Pascua
Nothofagus pumilio	NOPU	1766	1985	-40 20	-71 14	Chapelco
Nothofagus pumilio	NOPU	1604	2000	-39 53	-72 03	Choshuenco
Nothofagus pumilio	NOPU	1611	2000	-39 53	-72 03	Choshuenco2
Nothofagus pumilio	NOPU	1765	2000	-44 43	-71 27	Cisne
Nothofagus pumilio	NOPU	1546	1991	-41 16	-71 38	Co Diego de Leon
Nothofagus pumilio	NOPU	1759	2000	-54 47	-68 23	Co Martial
Nothofagus pumilio	NOPU	1731	1992	-47 10	-72 30	Co Tamango Inferior
Nothofagus pumilio	NOPU	1631	1992	-47 15	-72 30	Co Tamango Medio

Nothofagus pumilio	NOPU	1700	1995	-38 39	-71 37	Conguillo krumholz
Nothofagus pumilio	NOPU	1728	1996	-38 38	-71 36	Conguillo Lenga Abajo
Nothofagus pumilio	NOPU	1800	1996	-38 40	-71 37	Conguillo Lenga media
Nothofagus pumilio	NOPU	1819	1996	-50 48	-72 30	Contreras E
Nothofagus pumilio	NOPU	1793	1996	-50 48	-72 36	Contreras W
Nothofagus pumilio	NOPU	1726	1986	-54 26	-67 92	Ea Carmen Camino
Nothofagus pumilio	NOPU	1743	1986	-54 30	-67 05	Ea. Maria Cristina
Nothofagus pumilio	NOPU	1664	1984	-54 41	-67 50	Estacion Microondas
Nothofagus pumilio	NOPU	1793	1996	-53 38	-68 42	Estancia Las Flores
Nothofagus pumilio	NOPU	1723	1985	-54 03	-68 34	Estancia San Justo
Nothofagus pumilio	NOPU	1722	2000	-47 10	-72 30	Furioso
Nothofagus pumilio	NOPU	1595	1985	-41 10	-71 56	Glaciar Frias
Nothofagus pumilio	NOPU	1574	2000	-49 04	-72 54	Glaciar Huemules
Nothofagus pumilio	NOPU	1721	1998	-48 28	-72 15	Glaciar Narvaez 1
Nothofagus pumilio	NOPU	1606	1998	-48 29	-72 15	Glaciar Narvaez 2
Nothofagus pumilio	NOPU	1629	1998	-49 21	-72 58	Glaciar Piedras Blancas
Nothofagus pumilio	NOPU	1639	1986	-54 31	-67 25	Isla Grande Monticulo
Nothofagus pumilio	NOPU	1690	2000	-46 50	-72 06	Jeinimeni
Nothofagus pumilio	NOPU	1575	1984	-54 39	-67 52	Lago Escondido
Nothofagus pumilio	NOPU	1600	2000	-54 29	-69 07	Lago Fagnano 1
Nothofagus pumilio	NOPU	1647	1985	-45 00	-71 30	Lago Fontana
Nothofagus pumilio	NOPU	1731	1986	-54 28	-67 43	Lago Yehuin
Nothofagus pumilio	NOPU	1704	1995	-37 29	-71 20	Laja Las Cuevas
Nothofagus pumilio	NOPU	1728	1996	-37 34	-71 14	Laja Lenga Larga
Nothofagus pumilio	NOPU	1736	1996	-37 28	-71 19	Laja Los Barros
Nothofagus pumilio	NOPU	1731	1996	-53 22	-71 13	Monte Azul
Nothofagus pumilio	NOPU	1773	1996	-52 31	-71 01	Monte Gallina
Nothofagus pumilio	NOPU	1677	1988	-53 12	-72 10	Monte Grande Magallanes
Nothofagus pumilio	NOPU	1712	2000	-47 07	-71 54	Oportus
Nothofagus pumilio	NOPU	1692	1986	-40 40	-71 25	Paso Cordoba
Nothofagus pumilio	NOPU	1814	1991	-41 07	-71 48	Paso de las Nubes1
Nothofagus pumilio	NOPU	1662	1985	-54 39	-67 52	Paso Garibaldi
Nothofagus pumilio	NOPU	1718	1991	-41 07	-71 48	Paso de las Nubes 3
Nothofagus pumilio	NOPU	1701	1991	-41 07	-71 48	Paso de las Nubes 4
Nothofagus pumilio	NOPU	1850	1991	-41 07	-71 48	Paso de las Nubes 2
Nothofagus pumilio	NOPU	1662	1988	-53 30	-71 10	Peninsula Brunswick
Nothofagus pumilio	NOPU	1761	2000	-54 27	-68 42	Portezuelo fagnanoA-new
Nothofagus pumilio	NOPU	1709	2000	-54 26	-68 43	Portezuelo fagnanoB-new
Nothofagus pumilio	NOPU	1662	1998	-48 28	-72 09	Puesto Miraflores
Nothofagus pumilio	NOPU	1739	1986	-54 30	-67 48	Rio Claro
Nothofagus pumilio	NOPU	1705	1986	-54 31	-66 10	Rio Malenguena
Nothofagus pumilio	NOPU	1657	1984	-54 47	-68 28	Rio Pipo
Nothofagus pumilio	NOPU	1715	2000	-36 55	-71 25	Termas de Chillan
Nothofagus pumilio	NOPU	1650	2000	-49 19	-73 01	Torre
Nothofagus pumilio	NOPU	1703	2000	-49 19	-72 56	Torre Morena 4
Nothofagus pumilio	NOPU	1669	2000	-49 19	-72 59	Torre Norte
Nothofagus pumilio	NOPU	1674	2000	-49 20	-72 59	Torre Sur
Nothofagus pumilio	NOPU	1593	1984	-54 47	-68 11	Valle de Andorra
Nothofagus pumilio	NOPU	1611	2000	-49 25	-73 01	Valle Tunel
Nothofagus pumilio	NOPU	1819	1989	-35 36	-71 02	Vilches
Nothofagus pumilio	NOPU	1830	2000	-39 15	-72 15	Villarica
Nothofagus pumilio	NOPU	1811	1996	-54 57	-67 31	was.rwl
Pilgerodendron uviferum	PIUV	1597	2000	-53 32	-72 18	Bachelor
Pilgerodendron uviferum	PIUV	1554	2000	-53 49	-71 04	Bouchage
Pilgerodendron uviferum	PIUV	1400	2000	-53 39	-72 16	Carlos III
Pilgerodendron uviferum	PIUV	1518	2000	-42 45	-73 59	chrono 104
Pilgerodendron uviferum	PIUV	1770	2000	-43 03	-73 54	chrono 106
Pilgerodendron uviferum	PIUV	1462	2000	-47 42	-73 04	chrono 50
Pilgerodendron uviferum	PIUV	1741	2000	-43 59	-72 42	chrono 60
Pilgerodendron uviferum	PIUV	1464	1994	-44 19	-74 17	Laguna Facil
Pilgerodendron uviferum	PIUV	1437	2000	-48 02	-73 07	Laguna Leal
Pilgerodendron uviferum	PIUV	1755	1993	-46 09	-73 27	Laguna Miranda
Pilgerodendron uviferum	PIUV	1640	1994	-44 42	-73 45	Laguna Valentin
Pilgerodendron uviferum	PIUV	1595	2000	-48 55	-74 24	Moat Is.

Pilgerodendron uviferum	PIUV	1555	2000	-53 45	-71 00	Mount Tarn
Pilgerodendron uviferum	PIUV	1723	2000	-54 54	-70 00	Obriens Is.
Pilgerodendron uviferum	PIUV	1637	1994	-49 15	-74 05	Pio XI
Pilgerodendron uviferum	PIUV	1554	1987	-42 30	-73 50	Piuchue Is Chiloe
Pilgerodendron uviferum	PIUV	1543	2000	-49 06	-74 24	Puerto Eden
Pilgerodendron uviferum	PIUV	1460	1994	-40 44	-72 18	Puyehue* MERGE
Pilgerodendron uviferum	PIUV	1765	1982	-41 40	-71 25	Rio Foyel
Pilgerodendron uviferum	PIUV	1458	2000	-48 11	-73 09	Rio Pascua
Pilgerodendron uviferum	PIUV	1517	2000	-53 49	-71 07	San Nicolas
Pilgerodendron uviferum	PIUV	1400	2000	-39 36	-72 06	San Pablo
Pilgerodendron uviferum	PIUV	1677	2000	-53 45	-72 29	Santa Ines
Pilgerodendron uviferum	PIUV	1489	1986	-43 00	-72 30	Santa Lucia Chiloe
Pilgerodendron uviferum	PIUV	1530	2000	-53 40	-72 33	Seno Ballena
Pilgerodendron uviferum	PIUV	1400	2000	-48 42	-74 04	Tempano
Pilgerodendron uviferum	PIUV	1600	1993	-46 11	-73 34	Trails Top
Polylepis tarapacana	POTA	1400	2000	-18 58	-69 01	Cerro Capitan
Polylepis tarapacana	POTA	1573	2000	-22 13	-66 36	Cerro Ramada
Polylepis tarapacana	POTA	1431	2000	-22 00	-67 17	Cerro Soniquera
Polylepis tarapacana	POTA	1400	2000	-22 20	-67 14	Cerro Uturunco
Polylepis tarapacana	POTA	1400	2000	-19 07	-68 27	Frente Sabaya
Polylepis tarapacana	POTA	1400	2000	-20 43	-68 34	Irruputuncu
Polylepis tarapacana	POTA	1795	2000	-17 13	-69 13	Ja Condori+Cnic+serke+huari
Polylepis tarapacana	POTA	1761	2000	-17 56	-69 27	Nasahuento
Polylepis tarapacana	POTA	1444	2000	-19 22	-68 55	Queniza
Polylepis tarapacana	POTA	1484	2000	-18 56	-69 00	Surire High
Polylepis tarapacana	POTA	1400	2000	-18 54	-69 00	Surire Low
Polylepis tarapacana	POTA	1400	2000	-18 55	-69 00	Surire Medio
Polylepis tarapacana	POTA	1414	2000	-19 11	-68 54	Taipicollo
Polylepis tarapacana	POTA	1400	2000	-21 30	-67 52	Volcan Caquellas
Polylepis tarapacana	POTA	1620	2000	-22 35	-66 33	Volcan Granada + Cerro Negro
Polylepis tarapacana	POTA	1400	2000	-18 28	-69 10	Volcan Guallatire
Polylepis tarapacana	POTA	1650	2000	-18 35	-69 10	Volcan Guallatire_D
Prosopis ferox	PRFE	1853	2000	-23 08	-65 21	Quebrada Sapagua Humahuaca

Dataset S1. This record reports the scPDSI averages of the grid points from three regions (the Altiplano, central Chile and La Plata basin), and the occurrences of severe/extreme hidroclimate events reconstructed by historical information corresponding to the same regions.

Dataset S2. Estimators of ENSO (ENSO-e) and SAM (SAM-e) variability for the past 500 years obtained by MCA for reconstructed scPDSI fields from the SADA and ANZDA and the Sea Surface Temperature and Geopotential Height climate modes.

Dataset S3. The resulting time series of the difference between both climate index estimators (ENSO_e – SAM_e) and the anomalous negative/positive values by the 5th and 95th percentiles, respectively. 25 (26) negative (positive) values were associated with coupled anomalous negative (positive) ENSO-e and positive (negative) SAM-e events.

SI References

1. I. Harris, P. D. Jones, T. J. Osborn, D. H. Lister, Updated high-resolution grids of monthly climatic observations – the CRU TS3.10 Dataset. *Int. J. Climatol.* **34**, 623 – 642 (2014).
2. M. New, M. Hulme, P. D. Jones, Representing twentieth century space-time climate variability. Part II: Development of 1901-1996 monthly grids of terrestrial surface climate. *J. Climate* **13**, 2217-2238 (2000).
3. K. Matsuura, National Center for Atmospheric Research Staff. "The Climate Data Guide: Global (land) precipitation and temperature: Willmott & Matsuura, University of Delaware." Available at https://climatedataguide.ucar.edu/climate-data/global-land-precipitation-and-temperature-willmott-matsuura-university-delaware. Deposited 20 October 2017.
4. National Center for Atmospheric Research Staff. "The Climate Data Guide: GPCC: Global Precipitation Climatology Centre." Available at https://climatedataguide.ucar.edu/climate-data/gpcc-global-precipitation-climatology-centre. Deposited 20 September 2018.
5. E. R. Cook, K. J. Anchukaitis, B. M. Buckley, R. D'Arrigo, G. C. Jacoby, W. E. Wright, Asian monsoon failure and megadrought during the last millennium. *Science* **328**, 486–489 (2010).
6. N. Wells, S. Goddard, M. J. Hayes, A self-calibrating palmer drought severity index, J. Climate, **17**, 2335–2351, (2004).
7. H. C. Fritts, Tree rings and climate, (Academic Presss, London, 1976).
8. E. R. Cook, K. R. Briffa, D. M. Meko, D. A. Graybill, G. Funkhouser, The segment length curse in long tree-ring chronology development for paleoclimatic studies. *The Holocene* **5**, 229-237 (1995).
9. T. Melvin, K. Briffa, A 'signal-free' approach to dendroclimatic standardization, *Dendrochronologia* **26**, 71–86 (2008).
10. J. G. Palmer, E. R. Cook, C. S. M. Turney, K. Allen, P. Fenwick, B. I. Cook, A. O'Donnell, J. Lough, P. Grierson, P. Baker, Drought variability in the eastern Australia and New Zealand summer drought atlas (ANZDA, CE 1500–2012) modulated by the Interdecadal Pacific Oscillation. Environm. *Res. Lett.* **10**, 124002 (2015).
11. E. R. Cook, C. A. Woodhouse, C. M. Eakin, D. M. Meko, D. W. Stahle, Long-Term Aridity Changes in the Western United States. *Science* **306**, 1015-1018 (2004).
12. E. R. Cook, K. J. Anchukaitis, B. M. Buckley, R. D'Arrigo, G. C. Jacoby, W. E. Wright, Asian monsoon failure and megadrought during the last millennium. *Science* **328**, 486–489 (2010).
13. E. R. Cook, R. Seager, Y. Kushnir, K. R. Briffa, U. Büntgen, D. Frank, P. J. Krusic, W. Tegel, G. van der Schrier, L. Andreu-Hayles, M. Baillie, C. Baittinger, N. Bleicher, N. Bonde, D. Brown, M. Carrer, R. Cooper, K. Čufar, C. Dittmar, J. Esper, C. Griggs, B. Gunnarson, B. Günther, E. Gutierrez, K. Haneca, S. Helama, F. Herzig, K-U. Heussner, J. Hofmann, P. Janda, R. Kontic, N. Köse, T. Kyncl, T. Levanič, H. Linderholm, S. Manning, T. M. Melvin, D. Miles, B. Neuwirth, K. Nicolussi, P. Nola, M. Panayotov, I. Popa, A. Rothe, K. Seftigen, A. Seim, H. Svarva, M. Svoboda, T. Thun, M. Timonen, R. Touchan, V. Trotsiuk, V. Trouet, F.

Walder, T. Ważny, R. Wilson, C. Zang, Old World megadroughts and pluvials during the Common Era. *Sci. Adv.* **1,** e1500561 (2015).

14. E. R. Cook, D. M. Meko, D. W. Stahle, M. K. Cleaveland, Drought reconstructions for the continental United States. *J. Clim.* **12**, 1145-1162, (1999).
15. R. D. Garreaud, M. Vuille, R. Compagnucci, J. Marengo, Present day South American climate. *Palaeogeogr. Palaeoclim. Palaeocl.* **281**, 180–195 (2009).
16. J. Michaelsen, Cross-validation in statistical climate forecast models, *J. Clim. Appl. Meteorol.*, **26**, 1589–1600, (1987).
17. D. M., Meko, Dendroclimatic reconstruction with time varying subsets of tree indices, *J. Clim.* **10**, 687–696 (1997).
18. E. R Cook, O. Solomina, V. Matskovsky, B. I. Cook, L. Agafonov, E. Dolgova, A. Karpukhin, N. Knysh, M. Kulakova, V. Kuznetsova, T. Kyncl, J. Kyncl, O. Maximova, I. Panyushkina, A. Seim, D. Tishin, T. Wazny, M. Yermokhin. The European Russia Drought Atlas (1400-2016 CE). *Clim. Dyn.* https://doi.org/10.1007/s00382-019-05115-2 (2020).
19. M. R. Prieto, R. Garcia-Herrera, Documentary sources from South America: potential for climate reconstruction. *Palaeogeogr. Palaeocl. Palaeoecol.* **281**, 196–209 (2009).
20. A. Gioda, M. R. Prieto, Histoire des sécheresses andines: Potosi El Niño et le Petit Age Glaciaire, *La Météorologie* **8,** 33–42 (1999).
21. M. H. Masiokas, R. Villalba, D. A. Christie, E. Betman, B. H. Luckman, C. Le Quesne, M. R. Prieto, S. Mauget, Snowpack variations since AD 1150 in the Andes of Chile and Argentina (30°–37°S) inferred from rainfall, tree-ring and documentary records, *J. Geophys. Res.* **117**, D05112 (2012).
22. M. R. Prieto, R Herrera, P. Doussel, Historical evidences of streamflow fluctuations in the Mendoza River, Argentina, and their relationship with ENSO, *Holocene* **9**, 473–481 (1999).
23. M. R. Prieto, R. Herrera, T. Castrillejo, P. Doussel, Recent climatic variations and water availability in the central Andes of Argentina and Chile (1885–1996): The use of historical records to reconstruct climate (in Spanish), *Meteorologica* **25**, 27–43 (2000).
24. M. R. Prieto, R. Herrera, P. Doussel, L. Gimeno, P. Ribera, R. García, E. Hernández, Interannual oscillations and trend of snow occurrence in the Andes region since 1885, *Aust. Meteorol. Mag*. **50**, 164–168 (2001).
25. Ortlieb L., Major historical rainfalls in central Chile and the chronology of ENSO events during the XVI-XIX centuries, *Rev. Chil. Hist. Nat.* **67**, 463–485 (1994).
26. M.R. Prieto, ENSO signals in South America: Rains and floods in the Parana River during colonial times. *Climatic Change* **83**, 39-54 (2007)
27. National Center for Atmospheric Research Staff, "The Climate Data Guide: SST data: HadiSST v1.1." Available at https://climatedataguide.ucar.edu/climate-data/sst-data-hadisst-v11. Deposited 16 September 2019.
28. N. A. Rayner, D. E. Parker, E. B. Horton, C. K. Folland, L. V. Alexander, D. P. Rowell, E. C. Kent, A. Kaplan, Global analyses of sea surface temperature, sea ice, and night marine air temperature since the late nineteenth century *J. Geophys. Res.* **14**, 4407 10.1029/2002JD002670 (2002). Dataset available at https://climexp.knmi.nl/data/ihadisst1_nino3.4a.dat.
29. E. Kalnay, M. Kanamitsu, R. Kistler, W. Collins, D. Deaven, L. Gandin, M. Iredell, S. Saha, G. White, J. Woollen, Y. Zhu, M. Chelliah, W. Ebisuzaki, W. Higgins, J. Janowiak, K. C. Mo, C. Ropelewski, J. Wang, A. Leetmaa, R. Reynolds, R. Jenne, D. Joseph, The NCEP/NCAR 40-year reanalysis project, *Bull. Amer. Meteor. Soc.* **77**, 437-470 (1996). Dataset available at https://www.esrl.noaa.gov/psd/ i
30. British Antartic Survey. “An observation-based Southern Hemisphere Annular Mode Index”. Available at https://legacy.bas.ac.uk/met/gjma/sam.html. Deposited 14 January, 2020
31. G. J. Marshall, Trends in the southern annular mode from observations and reanalyses. *J. Clim.* **16**, 4134-4143 (2003).
32. E. R. Cook, R. D. D'Arrigo, K. J. Anchukaitis. Tree Ring 500 Year ENSO Index Reconstructions. *IGBP PAGES/World Data Center for Paleoclimatology Data Contribution Series # 2009-105*, (NOAA/NCDC Paleoclimatology Program, Boulder CO, USA, 2009).

33. J. Li, S.-P. Xie, E. R. Cook, , M. S. Morales, D. Christie, F. Chen, R. D'Arrigo, N. C. Johnson, A. M. Fowler, X. Gou, K. Fang, El Niño modulations during the past seven centuries, *Nat. Clim. Change* **3**, 822–826 (2013).
34. B. I. Cook, A. P. Williams, J. E. Smerdon, J. G. Palmer, E. R. Cook, D. W. Stahle, S. Coats, Cold tropical Pacific sea surface temperaturas during the late sixteenth-century North American megadrought. *J. Geophys. Res. Atmosph.* **123**, 11307–11320 (2018).
35. R. Wilson, E. Cook, R. D'Arrigo, N. Riedwyl, M. N. Evans, A. Tudhope, R. Allan,. Reconstructing ENSO: The influence of method, proxy data, climate forcing and teleconnections. *J. Quaternary Sci.* **25**, 62–78 (2010).
36. J. Emile-Geay, K. M. Cobb, M. E. Mann, A. T. Wittenberg, Estimating central equatorial Pacific SST variability over the past millennium. Part 2: Reconstructions and implications. *J. Clim.* **26**, 2329–2352 (2013).
37. R. Villalba, A. Lara, M. H. Masiokas, R. R. Urrutia, B. H. Luckman, G. J. Marshall, I. A. Mundo, D. A. Christie, E. R. Cook, R. Neukom, K. Allen, P. Fenwick, J. A. Boninsegna, A. M. Srur, M. S. Morales, D. Araneo, J. G. Palmer, E. Cuq, J. C. Aravena, A. Holz, C. LeQuesne, Unusual Southern Hemisphere tree growth patterns induced by changes in the southern annular mode. *Nat. Geosc.* **5**, 793–798 (2012).
38. N. J. Abram, R. Mulvaney, F. Vimeux, S. J. Phipps, J. Turner, M. H. England, Evolution of the Southern Annular Mode during the past millennium. *Nat. Clim. Change* **4**, 564–569 (2014).
39. C. Dätwyler, R. Neukom, N. J. Abram, A. J. E. Gallant, M. Grosjean, M. Jacques-Coper, D. J. Karoly, R. Villalba, Teleconnection stationarity, variability and trends of the Southern Annular Mode (SAM) during the last millennium. *Clim. Dyn.* **51**, 2321–2339 (2018).